Journal of Harbin Engineering University
ISSN: 1006-7043

Vol 45 No. 3
March 2024

Carreau Fluid Flow Towardsa Stagnation Region of Shrinking Sheet Containing Al2O3-Cu Hybrid Nanoparticles

IskandarWaini[1],KhairumBin Hamzah[2],NajiyahSafwaKhashi'ie[3], AnuarIshak[4], Ioan Pop[5]

[1, 2]FakultiTeknologidanKejuruteraanIndustridanPembuatan, UniversitiTeknikal Malaysia Melaka, Hang Tuah Jaya, Durian Tunggal 76100, Melaka, Malaysia

[3]FakultiTeknologidanKejuruteraanMekanikal, UniversitiTeknikal Malaysia Melaka, Hang Tuah Jaya, 76100 Durian Tunggal, Melaka, Malaysia

[4] Department of Mathematical Sciences, Faculty of Science and Technology, UniversitiKebangsaan Malaysia, 43600 UKM, Bangi, Selangor, Malaysia

[5] Department of Mathematics, Babes-Bolyai University, Romania

Abstract

This study investigates the hybrid nanofluid flow (Al2O3-Cu/water) on a stagnation region of a shrinking surface using the Carreau fluid model. The problem is solved by a similarity approach using appropriate similarity variables. Then, the bvp4c solver in MATLAB is employed to solve the similarity equations. The results show that two solutions are in existence in the shrinking region. Besides, the heat transfer rate at the surface increases in the presence of nanoparticles. Moreover, the increase of the power-law index as well as the Weissenberg number tends to increase the friction on the surface but decrease the heat transfer rate for the shrinking case.

Keywords:Hybrid nanofluid; Dual solutions; Carreau fluid, Stagnation flow, Shrinking sheet.

1. Introduction

The stagnation-point flow over a static flat surface was first investigated by Hiemenz[1]. Homann[2] then extended it to the axisymmetric flow case, and Wang [3] studied the flow toward a shrinking sheet. Apart from that, Mahapatra and Nandy[4] examined the problem on the porous shrinking sheet. They concluded that increasing the porosity extends the range of the solution domains. Moreover, Khashi'ie et al. [5] reported the effect of double stratification on the flow in a porous medium. Recently, Fang and Wang [6] investigated the stagnation flow over a moving surface, and successfully obtained the exact solution.

An advanced fluid named 'nanofluid' was introduced by Choi [7] to enhance the fluid's heat transfer rate in a cooling systems. Nanofluid contains suspended particles of nanosized in a base fluid. Several studies shown that there is a significant enhancement in the rate of heat transfer when more than one type of nanoparticles are added into the base liquid. The experiments done by Jana et al. [7] and Turcu et al. [8] are among the previous studies on the hybrid nanofluids. Suresh et al. [9] produced the Al_2O_3–Cu nanocomposite powder by employing the thermochemical method. They concluded that the addition of hybrid nanoparticles boosted the thermal conductivity of the fluid.

The hybrid nanofluid flow on a stretching surface was studied by Devi and Devi [10]. They developed the thermophysical correlations of the hybrid nanofluids. In that study, the correlations were compared and validated with those of Suresh et al. [9]. Similarly, Takabi and Salehi[11] reported that the desired level of heat transfer rate can be accomplished by considering the hybrid nanoparticles. It is worth mentioning that, the stability analysis of dual solutions on flow of a hybrid nanofluid along a shrinking surface was investigated by Waini et al. [12]. Since that several authors studied the effect of physical parameters on the hybrid nanofluid flow, for example, Waini et al. [13–16], Jaafar et al. [17], Tlili et al. [18], Jamaludin et al. [19], Roy et al. [20], Yasir et al. [21], Khan et al. [22,23], and Waqas et al. [24].For further reading,

comprehensive reviews on hybrid nanofluid are included in the review papers such asBabu et al. [25], Sidik et al. [26], Akilu et al. [27], and Huminic and Huminic[28].

The topic on flow analysis of non-Newtonian fluid has attracted the interest of the researchers nowadays. This is due to its promising application in industrial processes such as plastic foam processing, composite processing, bubble absorptions, and fermentation. Additionally, the non-Newtonian fluids flow originated by a moving surface are commonly involved in polymer and plastic extrusions, paper production, food processing, and many others. For example, the relationship of the constitutive expressions for Carreau fluid model sustains at both low and high shear rates. Historically, Carreau fluid model was first introduced by Carreau[29] in 1972. Then, this proposed model has been explored by the researchers to study fluid flow subject to diverse aspects, for example, Akbar et al. [30], Ganesh Kumar et al. [31], and Hayat et al. [32]. Besides, some researchers such as Bhatti et al. [33], Sulochana et al. [34], Rudraswamy et al. [35], and Ganesh Kumar et al. [36] investigated the Carreaunanofluid flow using the Buongiorno'snanofluid model. In addition, the study on Carreau fluid flow with nanoparticle effects has been investigated byMamathaUpadhya et al. [37], Ramana Reddy et al. [38], and Khan et al. [39] for several physical parameters. In these aforesaid studies, Carreau fluid model and Tiwari-Das nanofluid model were employed to formulate the problem. On the other hand, Megahed[40] studied the effect of thermal radiation and variable conductivity on Carreau fluid flow due to nonlinearly stretching sheet with variable heat flux.

Different from the above literature, the present study examines the flow in a stagnation region of a shrinking sheet where the effects of Al_2O_3-Cu hybrid nanoparticles are taken into consideration, using Carreau fluid model. In addition, the non-uniqueness of the solutions and their stabilities are investigated.

2. Mathematical Formulation

The stagnation point flow of Al_2O_3-Cu/water hybrid nanofluid over a stretching or a shrinking surface using the Carreau fluid model is considered. Figure 1 illustrates the flow configuration of the problem. We assume that the free stream and the surface velocities are given as $u_e(x) = ax/L$and $u_w(x) = bx/L$, respectively, where a and b are constant, and L is the reference length. The magnetic strength B_0 is executed along the *y*-axis. It is assumed that the surface temperature T_w and the ambient temperature T_∞ are constant.

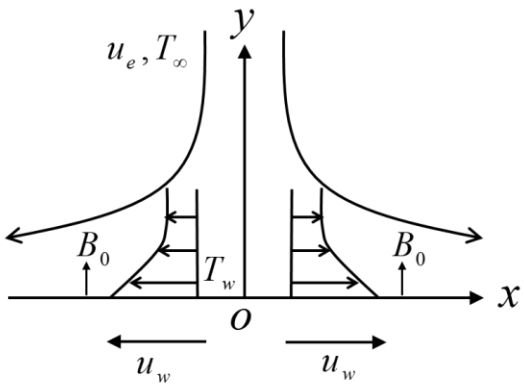

(a) Stretching sheet

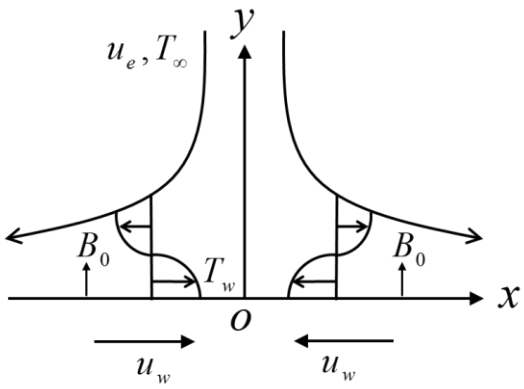

(b) Shrinking sheet

Fig. 1. Schematic Model

Based on these assumptions, the governing equations may be written as (see Devi and Devi [10]; Akbar et al. [30]; Ramana Reddy et al. [38]):

$$\frac{\partial u}{\partial x} + \frac{\partial v}{\partial y} = 0 \qquad (1)$$

$$u\frac{\partial u}{\partial x} + v\frac{\partial u}{\partial y} = u_e\frac{du_e}{dx} + \frac{\mu_{hnf}}{\rho_{hnf}}\left[\frac{\partial^2 u}{\partial y^2} + \frac{3}{2}(n-1)\Gamma^2\left(\frac{\partial u}{\partial y}\right)^2\frac{\partial^2 u}{\partial y^2}\right] - \frac{\sigma_{hnf}}{\rho_{hnf}}B_0^2(u-u_e) \qquad (2)$$

$$u\frac{\partial T}{\partial x} + v\frac{\partial T}{\partial y} = \frac{k_{hnf}}{(\rho C_p)_{hnf}}\frac{\partial^2 T}{\partial y^2} \qquad (3)$$

subject to:

$$v = 0, \quad u = u_w(x), \quad T = T_w \text{at} \quad y = 0$$
$$u \to u_e(x), \quad T \to T_\infty \text{ as} \quad y \to \infty \qquad (4)$$

where$u$ and$v$ are components velocity along the x- and y- axes. Besides, the temperature is given by T, n

represents the power-law index, and Γ represents the relaxation time with $\Gamma = (\Gamma_0/L)(x/L)^{-1}$where Γ_0 is a constant. Meanwhile, Table 1 [10] provides the thermophysical correlations of the hybrid nanofluid. Moreover, Table 2 [41,42] displays the properties of Al_2O_3, Cu, and water where φ_1 (Al_2O_3) and φ_2 (Cu) are the nanoparticles volume fractions.

To obtain similarity solution, the following dimensionless variables are considered (see Devi and Devi [10], Akbar et al. [30], and Ijaz and Ayub[43]):

$$\psi = \sqrt{\frac{a\nu_f}{L}}xf(\eta)\,, \quad \theta(\eta) = \frac{T-T_\infty}{T_w-T_\infty}, \quad \eta = y\sqrt{\frac{a}{L\nu_f}} \tag{5}$$

whereν_f is the fluid kinematic viscosity. As usually, the stream function ψ is defined as $u = \partial\psi/\partial y$and $v = -\partial\psi/\partial x$. Then, Eq. (1) is fully satisfied and we have:

$$u = \frac{ax}{L}f'(\eta), \qquad v = -\sqrt{\frac{a\nu_f}{L}}f(\eta) \tag{6}$$

Thus, Eqs. (2) and (3) become:

$$\frac{\mu_{hnf}/\mu_f}{\rho_{hnf}/\rho_f}\left[1+\frac{3}{2}(n-1)We^2f''^2\right]f''' + ff'' - f'^2 - \frac{\sigma_{hnf}/\sigma_f}{\rho_{hnf}/\rho_f}M^2(f'-1) + 1 = 0 \tag{7}$$

$$\frac{1}{\Pr}\frac{k_{hnf}/k_f}{(\rho C_p)_{hnf}/(\rho C_p)_f}\theta'' + f\theta' = 0 \tag{8}$$

subject to:

$$f(0) = 0, \quad f'(0) = \lambda, \quad \theta(0) = 1$$
$$f'(\infty) = 1, \quad \theta(\infty) = 0 \tag{9}$$

where the notation ′ means differentiation with respect to η, $\Pr = \mu_f(C_p)_f/k_f$ represents the Prandtl number, $We^2 = \Gamma_0^2a^3/L^3\nu_f$ represents the Weissenberg number, and $M^2 = \sigma_fB_0^2L/a\rho_f$ represents the magnetic parameter. Note that the stretching/shrinking parameter is defined by$\lambda = b/a$, where $\lambda > 0$ is for stretching, $\lambda < 0$ is for shrinking and $\lambda = 0$ indicates the static sheet. We note that, by taking $n = 1$or $We = 0$, this problem reduces to that of regular hybrid nanofluid flow. Thus, by considering Carreau hybrid nanofluid, we take the values of $n > 1$and $We > 0$.

The skin friction coefficient C_f and the local Nusselt number Nu_x are defined as:

$$C_f = \frac{\tau_w}{\rho_f u_e^2}, \quad Nu_x = \frac{xq_w}{k_f(T_w-T_\infty)} \tag{10}$$

withτ_w and q_w denote the shear stress and the heat flux from the surface, respectively, and defined as (see Akbar et al. [30]):

$$\tau_w = \mu_{hnf}\left(\frac{\partial u}{\partial y} + \frac{1}{2}(n-1)\Gamma^2\left(\frac{\partial u}{\partial y}\right)^3\right)_{y=0},$$
$$q_w = -k_{hnf}\left(\frac{\partial T}{\partial y}\right)_{y=0} \tag{11}$$

Using (5), (10) and (11), one gets:

$$Re_x^{1/2}C_f = \frac{\mu_{hnf}}{\mu_f}\left(f''(0) + \frac{1}{2}(n-1)We^2\left(f''(0)\right)^3\right),$$
$$Re_x^{-1/2}Nu_x = -\frac{k_{hnf}}{k_f}\theta'(0) \tag{12}$$

where$Re_x = u_ex/\nu_f$ is the local Reynolds number.

3. Stability Analysis

It is found that Eqs. (7) to (9) admit dual nature of solutions for a certain range of the physical parameters. A temporal stability analysis is done in order to determine the stability of the solutions in the long run. For this purpose, we follow the works of Merkin[44] and Weidman et al. [45]. Referring to Eqs. (5), the new variables are taken as:

$$\psi = \sqrt{\frac{a\nu_f}{L}}xf(\eta,\tau)\,, \quad \theta(\eta,\tau) = \frac{T-T_\infty}{T_w-T_\infty},$$
$$\eta = y\sqrt{\frac{a}{L\nu_f}} \qquad \tau = \frac{at}{L} \tag{13}$$

Now, using (13) and the unsteady form of Eqs. (2) to (3), one obtains:

$$\frac{\mu_{hnf}/\mu_f}{\rho_{hnf}/\rho_f}\left[1+\frac{3}{2}(n-1)We^2\left(\frac{\partial^2 f}{\partial\eta^2}\right)^2\right]\frac{\partial^3 f}{\partial\eta^3} + f\frac{\partial^2 f}{\partial\eta^2} - \left(\frac{\partial f}{\partial\eta}\right)^2 - \frac{\sigma_{hnf}/\sigma_f}{\rho_{hnf}/\rho_f}M^2\left(\frac{\partial f}{\partial\eta}-1\right) + 1 - \frac{\partial^2 f}{\partial\eta\partial\tau} = 0 \tag{14}$$

$$\frac{1}{\Pr}\frac{k_{hnf}/k_f}{(\rho C_p)_{hnf}/(\rho C_p)_f}\frac{\partial^2\theta}{\partial\eta^2} + f\frac{\partial\theta}{\partial\eta} - \frac{\partial\theta}{\partial\tau} = 0 \tag{15}$$

subject to:

$$f(0,\tau) = 0, \qquad \frac{\partial f}{\partial\eta}(0,\tau) = \lambda, \quad \theta(0,\tau) = 1$$
$$\frac{\partial f}{\partial\eta}(\infty,\tau) = 1, \quad \theta(\infty,\tau) = 0 \tag{16}$$

Following Weidman et al.[45], the steady solution $f = f_0(\eta)$ and $\theta = \theta_0(\eta)$ of Eqs. (7) - (9) are perturbed as follows:

$$f(\eta,\tau) = f_0(\eta) + e^{-\gamma\tau}F(\eta),$$
$$\theta(\eta,\tau) = \theta_0(\eta) + e^{-\gamma\tau}G(\eta) \tag{17}$$

where$F(\eta)$ and $G(\eta)$ are small compared to $f_0(\eta)$ and $\theta_0(\eta)$. Here, the sign of the eigenvalue γ will determine the stability of the solutions. By employing Eq. (17), and after linearization, Eqs. (14) and (15) become:

$$\frac{\mu_{hnf}/\mu_f}{\rho_{hnf}/\rho_f}\left[1+\frac{3}{2}(n-1)We^2 f_0^{''2}\right]F''' + 3\frac{\mu_{hnf}/\mu_f}{\rho_{hnf}/\rho_f}(n-1)We^2 f_0'' F'' f_0''' + f_0 F'' + f_0'' F - 2f_0' F' - \frac{\sigma_{hnf}/\sigma_f}{\rho_{hnf}/\rho_f}M^2 F' + \gamma F' = 0 \quad (18)$$

$$\frac{1}{\Pr}\frac{k_{hnf}/k_f}{(\rho C_p)_{hnf}/(\rho C_p)_f}G'' + f_0 G' + \theta_0' F + \gamma G = 0 \quad (19)$$

subject to:

$$F(0)=0,\quad F'(0)=0,\quad G(0)=0$$
$$F'(\infty)=0,\quad G(\infty)=0 \quad (20)$$

Following Harris et al. [46], without loss of generality we obtain γ in Eqs. (18) and (19) by setting $F''(0)=1$.

Table1. Thermophysical properties of nanoparticles and water

Properties	**Nanoparticles**		**Base fluid**
	Al_2O_3	Cu	water
$\rho\ (kg/m^3)$	2810	2720	792
$C_p\ (J/kgK)$	960	893	2545
$k\ (W/mK)$	173	222	0.2035
$\sigma\ (S/m)$	26.77×10^6	34.83×10^6	0.5×10^{-6}
Pr			7.38

Table 2.Thermophysical properties of hybrid nanofluid

Thermophysical properties	**Hybrid Nanofluid**
Density	$\rho_{hnf}=(1-\varphi_2)\left[(1-\varphi_1)\rho_f+\varphi_1\rho_{n1}\right]+\varphi_2\rho_{n2}$
Heat capacity	$(\rho C_p)_{hnf}=(1-\varphi_2)\left[(1-\varphi_1)(\rho C_p)_f+\varphi_1(\rho C_p)_{n1}\right]+\varphi_2(\rho C_p)_{n2}$
Dynamic viscosity	$\frac{\mu_{hnf}}{\mu_f}=\frac{1}{(1-\varphi_1)^{2.5}(1-\varphi_2)^{2.5}}$
Thermal conductivity	$\frac{k_{hnf}}{k_{nf}}=\frac{k_{n2}+2k_{nf}-2\varphi_2(k_{nf}-k_{n2})}{k_{n2}+2k_{nf}+\varphi_2(k_{nf}-k_{n2})}$ where $\frac{k_{nf}}{k_f}=\frac{k_{n1}+2k_f-2\varphi_1(k_f-k_{n1})}{k_{n1}+2k_f+\varphi_1(k_f-k_{n1})}$
Electrical conductivity	$\frac{\sigma_{hnf}}{\sigma_{nf}}=\frac{\sigma_{n2}+2\sigma_{nf}-2\varphi_2(\sigma_{nf}-\sigma_{n2})}{\sigma_{n2}+2\sigma_{nf}+\varphi_2(\sigma_{nf}-\sigma_{n2})}$ where $\frac{\sigma_{nf}}{\sigma_f}=\frac{\sigma_{n1}+2\sigma_f-2\varphi_1(\sigma_f-\sigma_{n1})}{\sigma_{n1}+2\sigma_f+\varphi_1(\sigma_f-\sigma_{n1})}$

4. Results and Discussion

Equations (7) to (9) are solved by utilising the function bvp4c in MATLAB software. The details procedure are described in [47]. Table 3 provides the values of $f''(0)$ when $\varphi_1=\varphi_2=0$ (regular fluid), $We=M=0$ and $n=1$ for different values of λ. Note that the present numerical values of $f''(0)$are comparable with those obtained by Wang [3], Mahapatra and Nandy[4], Khashi'ie et al. [5], and Akbar et al. [30]. The values of $Re_x^{1/2}C_f$ and $Re_x^{-1/2}Nu_x$ when $\Pr=6.2$ under several physical parameters for Cu/water $(\varphi_1=0)$ and Al_2O_3-Cu/water $(\varphi_1=0.1)$are calculated and presented in Table 4. We see that the values of $Re_x^{1/2}C_f$ accelerate with the rise of φ_2, n, We and M, whereas it decelerates with the increasing of λ. Meanwhile, the increasing of φ_2, M, and λ tends to boost the values of $Re_x^{-1/2}Nu_x$, while it reduces with n, and We. It is also

noticed that the values of $Re_x^{-1/2}Nu_x$are intensified for Al_2O_3-Cu/water.

The variations of $Re_x^{1/2}C_f$ and $Re_x^{-1/2}Nu_x$ against λ for several physical parameters are illustrated in Figs. 2 to 7. Based on our computations, the solutions are not unique for $\lambda_c < \lambda \leq -1.1$. No similarity solution was obtained when $\lambda < \lambda_c$. Besides, the critical values λ_c are located almost at the same point for each value of parameters considered. Separately, Figs. 2 and 3 display the variations of $Re_x^{1/2}C_f$ and $Re_x^{-1/2}Nu_x$ againstλ when $n = 2, We = M = \varphi_1 = 0.1$ and$\Pr = 6.2$ for different values of φ_2. It is discovered that $\lambda_c = -1.2554$, -1.2547, and $-1.2542$for $\varphi_2 = 0.01$, 0.05 and 0.1, respectively. Also, the heat transfer rate $Re_x^{-1/2}Nu_x$ enhances with the rising of φ_2, whereas the skin friction coefficient $Re_x^{1/2}C_f$decreases when $\lambda > 1$, increases when $\lambda < 1$, and no friction occurs when $\lambda = 1$ for the upper branch solutions. Meanwhile, there are no significant changes is seen for the second solutions. Figures 4 and 5 show the effect of n on $Re_x^{1/2}C_f$ and $Re_x^{-1/2}Nu_x$ against$\lambda$when $We = 0.5, M = \varphi_1 = \varphi_2 = 0.1$, and $\Pr = 6.2$. The critical values for $n = 1$ are $\lambda_{c1} = -1.2541$, $n = 2$ is$\lambda_{c2} = -1.2559$, and $n = 4$ is$\lambda_{c3} = -1.2576$. Moreover, the influence of Weon $Re_x^{1/2}C_f$ and $Re_x^{-1/2}Nu_x$ againstλ when $\Pr = 6.2, n = 2, M = \varphi_1 = \varphi_2 = 0.1$ are portrayed in Figs. 6 and 7. The critical values for $We = 0.1, 0.5,$ and 1 are $\lambda_c = -1.2542, -1.2559,$ and -1.2582, respectively. From these figures, the increasing of $n$and Welead to upsurge the values of $Re_x^{1/2}C_f$ but decrease the values of $Re_x^{-1/2}Nu_x$ for the shrinking sheet case.

Further, some samples of velocity $f'(\eta)$and temperature $\theta(\eta)$profiles for different values of parameters are presented in Figs. 8 - 13. These profiles satisfy the free stream conditions (9) asymptotically, thus support the validity of the numerical outcomes. The rise of φ_2 tends to upsurge the values of $f'(\eta)$, whereas $\theta(\eta)$ decreases for both branches when $\Pr = 6.2, \lambda = -1.2, n = 2, We = M = \varphi_1 = 0.1$as shown in Figs. 8 and 9. Moreover, Figs. 10 and 11 describe the effect of power-law index n on $f'(\eta)$and $\theta(\eta)$. It shows that when we consider $\Pr = 6.2, \lambda = -1.2, We = 0.5, M = \varphi_1 = \varphi_2 = 0.1$, the profiles of$f'(\eta)$ show the decreasing behaviour with an increase of n, meanwhile, it leads to upsurge the temperature $\theta(\eta)$ for both branches. Meanwhile, the features are similar for Weissenberg number We effects on $f'(\eta)$ and $\theta(\eta)$ when $\Pr = 6.2, \lambda = -1.2, n = 2, M = \varphi_1 = \varphi_2 = 0.1$ as seen in Figs. 12 and 13.

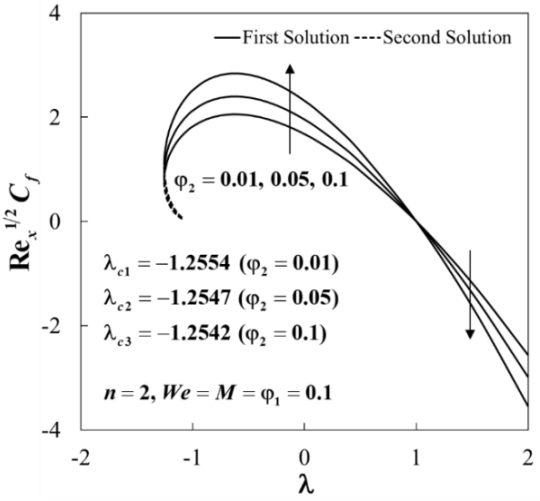

Fig. 2.$Re_x^{1/2}C_f$ vsλ for different φ_2

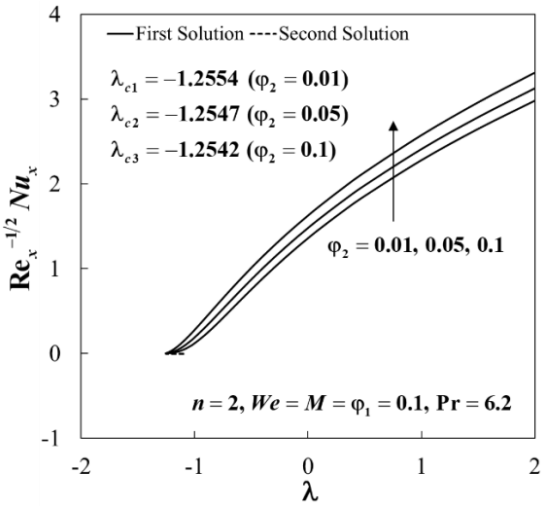

Fig. 3.$Re_x^{-1/2}Nu_x$ vs λ for different φ_2

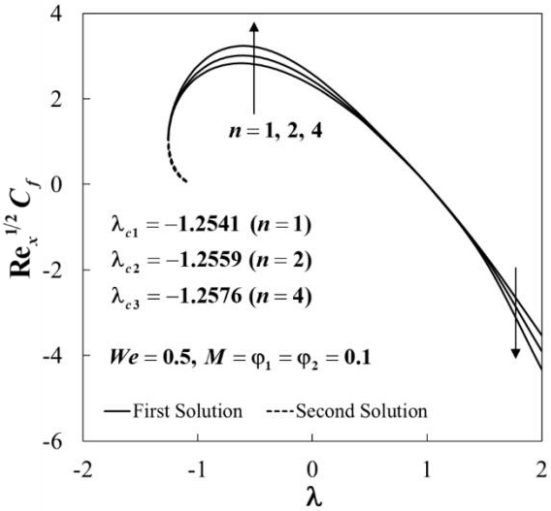

Fig. 4.$Re_x^{1/2}C_f$ vs λ and *n*

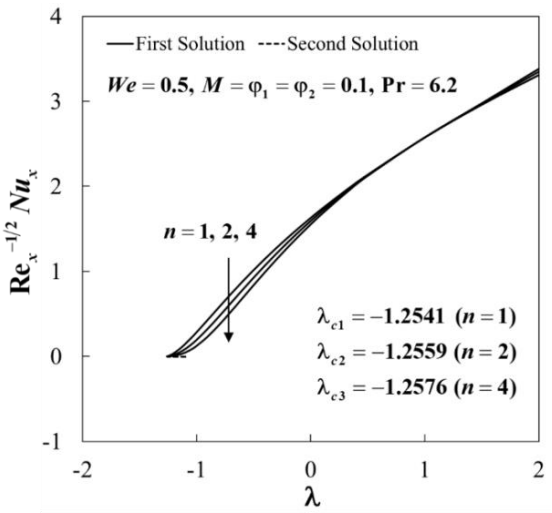

Fig. 5.$Re_x^{-1/2}Nu_x$ vsλ and n

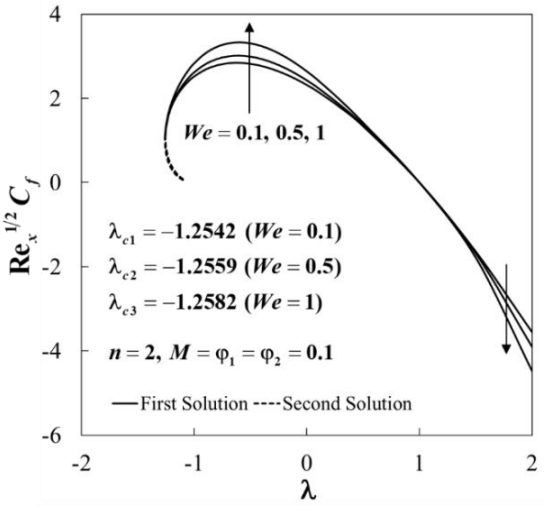

Fig. 6.$Re_x^{1/2}C_f$vsλ for different We

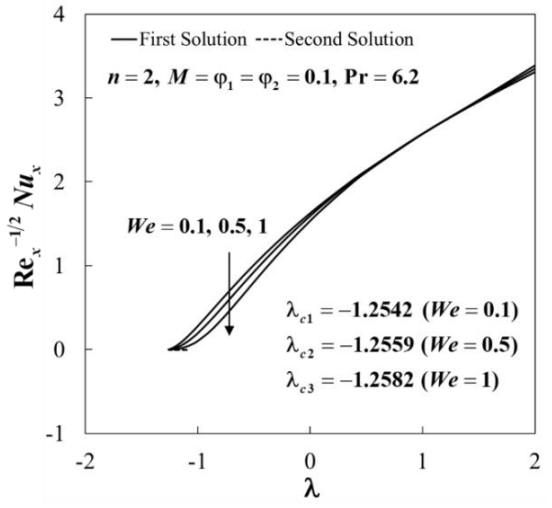

Fig. 7.$Re_x^{-1/2}Nu_x$ vsλ for different We

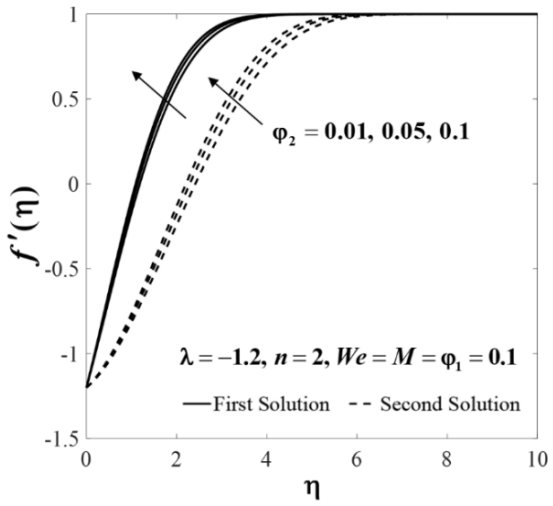

Fig. 8. Velocity $f'(\eta)$ vs η andφ_2

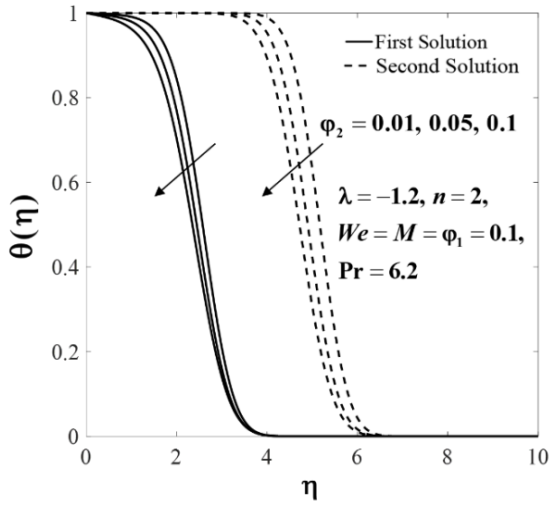

Fig. 9. Temperature $\theta(\eta)$ vs η andφ_2

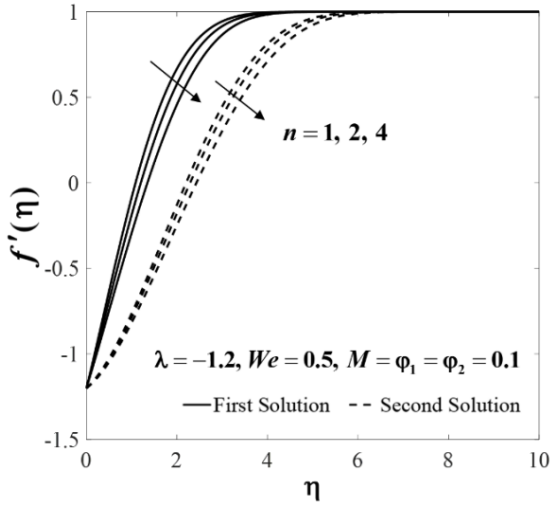

Fig. 10. Velocity $f'(\eta)$ vs η and n

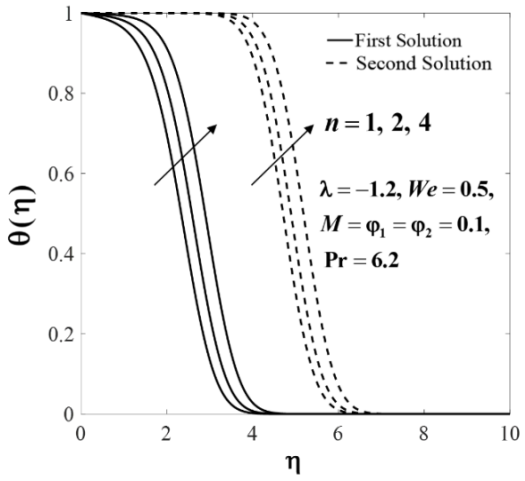

Fig. 11. Temperature $\theta(\eta)$ vs η and n

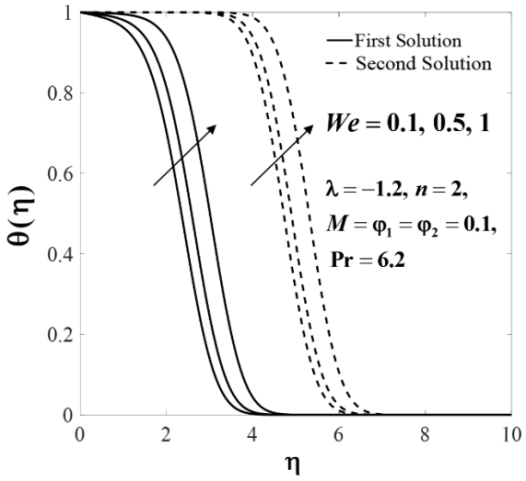

Fig. 13. Temperature $\theta(\eta)$ vs η and We

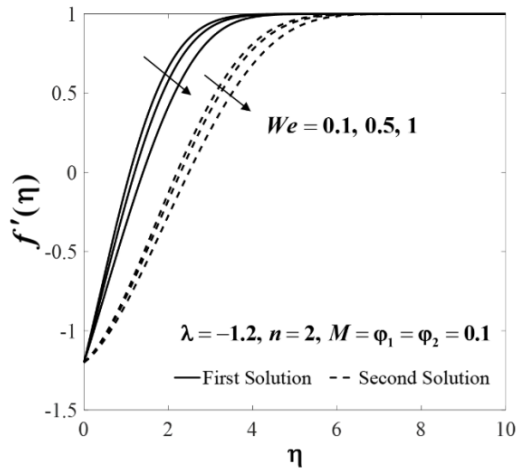

Fig. 12. Velocity $f'(\eta)$ vs η and We

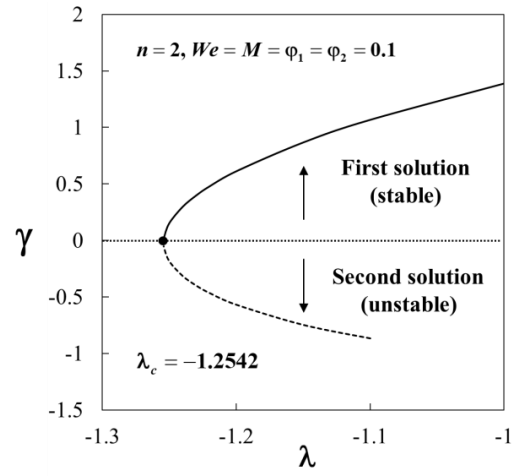

Fig. 14. Smallest eigenvalues γ against λ

Table 3. Comparison values of $f''(0)$when $\varphi_1 = \varphi_2 = 0$, $We = M = 0$ and $n = 1$ for different values of λ.

λ	Wang [3]	Mahapatra and Nandy[4]	Khashi'ie et al. [5]	Akbar et al. [30]	Present results
2	-1.88731				-1.88731
1	0	0	0	0	0
0.5	0.71330	0.7133	0.713295	0.7133	0.713295
0	1.232588	1.2326	1.232588	1.2326	1.232588
-0.25	1.40224	1.4022		1.4022	1.402241
-0.5	1.49567	1.4957	1.495670	1.4957	1.495670
-0.75	1.48930	1.4893		1.4893	1.489298
-1	1.32882	1.3288	1.328817	1.3288	1.328817
-1.1		1.1867 [0.0492]		1.1867 [0.0492]	1.186680 [0.049229]
-1.15	1.08223 [0.116702]	1.0822 [0.1167]		1.0822 [0.1167]	1.082231 [0.116702]
-1.2		0.9324 [0.2336]	0.932473 [0.23365]	0.9325 [0.2336]	0.932473 [0.233650]

Note: Results in "[ ]" are the second solutions.

Table 4 Values of $Re_x^{1/2}C_f$ and $Re_x^{-1/2}Nu_x$ when $\mathbf{Pr} = 6.2$ for different physical parameters

					Cu/water ($\varphi_1 = 0$)		Al_2O_3-Cu/water ($\varphi_1 = 0.1$)	
φ_2	n	We	M	λ	$Re_x^{1/2}C_f$	$Re_x^{-1/2}Nu_x$	$Re_x^{1/2}C_f$	$Re_x^{-1/2}Nu_x$
0.01	1	0	0	0	1.296890	1.157073	1.669493	1.360988
0.05	1	0	0	0	1.553850	1.269379	1.943879	1.480786
0.1	1	0	0	0	1.884324	1.404327	2.304578	1.627904
0.1	2	1	0	0	2.181486	1.315378	2.638018	1.534833
0.1	3	1	0	0	2.350729	1.276221	2.832687	1.491884
0.1	4	1	0	0	2.478018	1.250229	2.980083	1.462976
0.1	2	0.1	0	0	1.889376	1.402470	2.310042	1.626069
0.1	2	0.5	0	0	1.987521	1.369383	2.418261	1.592387
0.1	2	1	0	0	2.181486	1.315378	2.638018	1.534833
0.1	2	1	0.1	0	2.187691	1.315916	2.646652	1.535554
0.1	2	1	0.5	0	2.333779	1.328162	2.849290	1.551793
0.1	2	1	1	0	2.761468	1.359866	3.436924	1.592774
0.1	2	1	1	-0.5	3.855599	0.739206	4.838987	0.931330
0.1	2	1	1	0	2.761468	1.359866	3.436924	1.592774
0.1	2	1	1	0.5	1.386257	1.871738	1.721980	2.141692

The variations of γ against $\lambda$when $n = 2, We = M = \varphi_1 = \varphi_2 = 0.1$ are portrayed in Fig. 14. By the definition in Eq. (17), as time evolves ($\tau \to \infty$),$e^{-\gamma\tau} \to 0$ for positive values of γ but $e^{-\gamma\tau} \to \infty$ for the negative counterpart. These behaviours show that the first solution approaches the steady-state solution, which implies that the first solution is stable, but the second solution is unstable in the long run and thus not physically relevant.

5. Conclusion

The flow on a stagnation region of a shrinking sheet using Carreau fluid model containing hybrid nanoparticles was accomplished. The effects of the involved parameters on the flow behaviour were investigated. The numerical outcomes showed that the heat transfer rate of Al_2O_3-Cu/water intensified than Cu/water counterpart. We found that the solutions are not unique for the shrinking strength $\lambda_c < \lambda \leq -1.1$. The effect of φ_2 led to increase the local Nusselt number$Re_x^{-1/2}Nu_x$. There was no friction at the fluid-sheet interface when $\lambda = 1$ since the fluid and the sheet move with the same velocity for this case. Meanwhile, the increasing of $n$and Weled to increase the skin friction $Re_x^{1/2}C_f$ but decrease the local Nusselt number $Re_x^{-1/2}Nu_x$ for the shrinking case.An increment in $f'(\eta)$ was observed, whereas $\theta(\eta)$ decreased with the rise of $\varphi_2$for both branches of solutions. The increasing of n and We tended to increase the temperature $\theta(\eta)$ but to decrease the velocity$f'(\eta)$ for both branches. Between the two solutions, only one of them is stable over time.

6. Acknowledgement

A grateful acknowledgement goes to UniversitiTeknikal Malaysia Melaka, UniversitiTeknologi MARA, and UniversitiKebangsaan Malaysia. This research was funded by UniversitiTeknikal Malaysia Melaka (JURNAL/2019/FTKMP/ Q00042).

References

[1] K. Hiemenz, Die Grenzschicht an einem in den gleichförmigenFlüssigkeitsstromeingetauchteng eradenKreiszylinder, DinglersPolytechnisches Journal 326 (1911) 321–410.

[2] F. Homann, Der EinflubgroberZähigkeitbei der Strömung um den Zylinder und um die Kugel, Z Angew Math Mech 16 (1936) 153–164.

[3] C.Y. Wang, Stagnation flow towards a shrinking sheet, Int J Non Linear Mech 43 (2008) 377–382. https://doi.org/10.1016/j.ijnonlinmec.2007.12.021.

[4] T.R. Mahapatra, S.K. Nandy, Stability of dual solutions in stagnation-point flow and heat transfer over a porous shrinking sheet with thermal radiation, Meccanica 48 (2013) 23–32.

[5] N.S. Khashi'ie, N.Md. Arifin, M.M. Rashidi, E.H. Hafidzuddin, N. Wahi, Magnetohydrodynamics (MHD) stagnation point flow past a shrinking/stretching surface with double stratification effect in a porous medium, J Therm Anal Calorim 8 (2019) 1–14.

[6] T.G. Fang, F.J. Wang, Momentum and heat transfer of a special case of the unsteady stagnation-point flow, Appl Math Mech 41 (2020) 51–82.

[7] S. Jana, A. Salehi-Khojin, W.H. Zhong, Enhancement of fluid thermal conductivity by the addition of single and hybrid nano-additives, ThermochimActa 462 (2007) 45–55.

[8] R. Turcu, A. Darabont, A. Nan, N. Aldea, D. Macovei, D. Bica, L. Vekas, O. Pana, M.L. Soran, A.A. Koos, L.P. Biro, New polypyrrole-multiwall carbon nanotubes hybrid materials, Journal of Optoelectronics and Advanced Materials 8 (2006) 643–647.

[9] S. Suresh, K.P. Venkitaraj, P. Selvakumar, M. Chandrasekar, Synthesis of Al2O3-Cu/water hybrid nanofluids using two step method and its thermo physical properties, Colloids Surf A PhysicochemEng Asp 388 (2011) 41–48.

[10] S.P.A. Devi, S.S.U. Devi, Numerical investigation of hydromagnetic hybrid Cu- Al2O3/water nanofluid flow over a permeable stretching sheet with suction, International Journal of Nonlinear Sciences and Numerical Simulation 17 (2016) 249–257.

[11] B. Takabi, S. Salehi, Augmentation of the heat transfer performance of a sinusoidal corrugated enclosure by employing hybrid nanofluid, Advances in Mechanical Engineering 6 (2014) 147059.

[12] I. Waini, A. Ishak, I. Pop, Unsteady flow and heat transfer past a stretching/shrinking sheet in a hybrid nanofluid, Int J Heat Mass Transf 136 (2019) 288–297.

[13] I. Waini, A. Ishak, I. Pop, Hybrid nanofluid flow on a shrinking cylinder with prescribed surface heat flux, Int J Numer Methods Heat Fluid Flow 31 (2021) 1987–2004.

[14] I. Waini, A. Ishak, I. Pop, Hybrid nanofluid flow over a permeable non-isothermal shrinking surface, Mathematics 9 (2021) 538.

[15] I. Waini, A. Ishak, I. Pop, Symmetrical solutions of hybrid nanofluid stagnation-point flow in a porous medium, International Communications in Heat and Mass Transfer 130 (2022) 105804.

[16] I. Waini, U. Khan, A. Zaib, A. Ishak, I. Pop, Inspection of TiO2-CoFe2O4 nanoparticles on MHD flow toward a shrinking cylinder with radiative heat transfer, J MolLiq 361 (2022).

[17] A. Jaafar, I. Waini, A. Jamaludin, R. Nazar, I. Pop, MHD flow and heat transfer of a hybrid nanofluid past a nonlinear surface stretching/shrinking with effects of thermal radiation and suction, Chinese Journal of Physics 79 (2022) 13–27.

[18] I. Tlili, H.A. Nabwey, G.P. Ashwinkumar, N. Sandeep, 3-D magnetohydrodynamic AA7072-AA7075/methanol hybrid nanofluid flow above an uneven thickness surface with slip effect, Sci Rep 10 (2020) 1–13.

[19] A. Jamaludin, R. Nazar, K. Naganthran, I. Pop, Mixed convection hybrid nanofluid flow over an exponentially accelerating surface in a porous media, Neural ComputAppl 33 (2022) 15719–15729.

[20] N.C. Roy, A. Hossain, I. Pop, Flow and heat transfer of MHD dusty hybrid nanofluids over a shrinking sheet, Chinese Journal of Physics 77 (2022) 1342–1356.

[21] M. Yasir, M. Sarfraz, M. Khan, A.K. Alzahrani, M.Z. Ullah, Estimation of dual branch solutions for Homann flow of hybrid nanofluid towards biaxial shrinking surface, J Pet SciEng 218 (2022) 110990.

[22] U. Khan, A. Zaib, A. Ishak, I. Waini, Z. Raizah, B.C. Prasannakumara, A.M. Galal, Dynamics of bio-convection Agrawal axisymmetric flow of water-based Cu-TiO2 hybrid nanoparticles through a porous moving disk with zero mass flux, ChemPhys 561 (2022) 111599.

[23] U. Khan, A. Zaib, A. Ishak, I. Waini, A.-H. Abdel-Aty, M.A. Sheremet, I.S. Yahia, H.Y. Zahran,

A.M. Galal, Agrawal Axisymmetric Rotational Stagnation-Point Flow of a Water-Based Molybdenum Disulfide-Graphene Oxide Hybrid Nanofluid and Heat Transfer Impinging on a Radially Permeable Moving Rotating Disk, Nanomaterials 12 (2022) 787.

[24] H. Waqas, S. Ali Khan, T. Muhammad, Thermal analysis of magnetized flow of AA7072-AA7075/blood-based hybrid nanofluids in a rotating channel, Alexandria Engineering Journal 61 (2022) 3059–3068.

[25] J.A.R. Babu, K.K. Kumar, S.S. Rao, State-of-art review on hybrid nanofluids, Renewable and Sustainable Energy Reviews 77 (2017) 551–565.

[26] N.A.C. Sidik, I.M. Adamu, M.M. Jamil, G.H.R. Kefayati, R. Mamat, G. Najafi, Recent progress on hybrid nanofluids in heat transfer applications: A comprehensive review, International Communications in Heat and Mass Transfer 78 (2016) 68–79.

[27] S. Akilu, K. V. Sharma, A.T. Baheta, R. Mamat, A review of thermophysical properties of water based composite nanofluids, Renewable and Sustainable Energy Reviews 66 (2016) 654–678.

[28] G. Huminic, A. Huminic, Hybrid nanofluids for heat transfer applications – A state-of-the-art review, Int J Heat Mass Transf 125 (2018) 82–103.

[29] P.J. Carreau, Rheological Equations From Molecular Network Theories, Transactions of the Society of Rheology 16 (1972) 99–127.

[30] N.S. Akbar, S. Nadeem, R.U. Haq, S. Ye, MHD stagnation point flow of Carreau fluid toward a permeable shrinking sheet: Dual solutions, Ain Shams Engineering Journal 5 (2014) 1233–1239.

[31] K. Ganesh Kumar, B.J. Gireesha, N.G. Rudraswamy, S. Manjunatha, Radiative heat transfers of Carreau fluid flow over a stretching sheet with fluid particle suspension and temperature jump, Results Phys 7 (2017) 3976–3983.

[32] T. Hayat, I. Ullah, B. Ahmad, A. Alsaedi, Radiative flow of Carreau liquid in presence of Newtonian heating and chemical reaction, Results Phys 7 (2017) 715–722.

[33] M. Bhatti, T. Abbas, M. Rashidi, M. Ali, Numerical simulation of entropy generation with thermal radiation on MHD Carreaunanofluid towards a shrinking sheet, Entropy 18 (2016) 200.

[34] C. Sulochana, G.P. Ashwinkumar, N. Sandeep, Transpiration effect on stagnation-point flow of a Carreaunanofluid in the presence of thermophoresis and Brownian motion, Alexandria Engineering Journal 55 (2016) 1151–1157.

[35] N.G. Rudraswamy, S.A. Shehzad, K. Ganesh Kumar, B.J. Gireesha, Numerical analysis of MHD three-dimensional Carreaunanoliquid flow over bidirectionally moving surface, Journal of the Brazilian Society of Mechanical Sciences and Engineering 39 (2017) 5037–5047.

[36] K. Ganesh Kumar, G.K. Ramesh, B.J. Gireesha, A.M. Rashad, On stretched magnetic flow of Carreaunanofluid with slip effects and nonlinear thermal radiation, Nonlinear Engineering 8 (2019) 340–349.

[37] S. MamathaUpadhya, Mahesha, C.S.K. Raju, Unsteady flow of Carreau fluid in a suspension of dust and graphene nanoparticles with Cattaneo-Christov heat flux, J Heat Transfer 140 (2018) 092401.

[38] J. V. Ramana Reddy, V. Sugunamma, N. Sandeep, Simultaneous impacts of Joule heating and variable heat source/sink on MHD 3D flow of Carreau-nanoliquids with temperature dependent viscosity, Nonlinear Engineering 8 (2019) 356–367.

[39] N.S. Khan, T. Gul, P. Kumam, Z. Shah, S. Islam, W. Khan, S. Zuhra, A. Sohail, Influence of inclined magnetic field on Carreaunanoliquid thin film flow and heat transfer with graphene nanoparticles, Energies (Basel) 12 (2019) 1459.

[40] A.M. Megahed, Carreau fluid flow due to nonlinearly stretching sheet with thermal radiation, heat flux, and variable conductivity, Applied Mathematics and Mechanics (English Edition) 40 (2019) 1615–1624.

[41] H.F. Oztop, E. Abu-Nada, Numerical study of natural convection in partially heated rectangular enclosures filled with nanofluids, Int J Heat Fluid Flow 29 (2008) 1326–1336.

[42] J. Raza, A. Rohni, Z. Omar, Numerical investigation of copper-water (Cu-water) nanofluid with different shapes of nanoparticles in a channel with stretching wall: Slip effects, Mathematical and Computational Applications 21 (2016) 43.

[43] M. Ijaz, M. Ayub, Activation energy and dual stratification effects for Walter-B fluid flow in view of Cattaneo-Christov double diffusionon, Heliyon 5 (2019) e01815.

[44] J.H. Merkin, On dual solutions occurring in mixed convection in a porous medium, J Eng Math 20 (1986) 171–179.

[45] P.D. Weidman, D.G. Kubitschek, A.M.J. Davis, The effect of transpiration on self-similar boundary layer flow over moving surfaces, Int J EngSci 44 (2006) 730–737.

[46] S.D. Harris, D.B. Ingham, I. Pop, Mixed convection boundary-layer flow near the stagnation point on a vertical surface in a porous medium: Brinkman model with slip, Transp Porous Media 77 (2009) 267–285.

[47] L.F. Shampine, I. Gladwell, S. Thompson, Solving ODEs with MATLAB, Cambridge University Press, Cambridge, 2003.